

Continental interior storm tracks, tritium deposition, and precipitation isotopes at the Great Basin-Rocky Mountain physiographic provinces transition zone, USA

Alan Mayo¹ and David Tingey²

¹Mayo and Associates LLC

²Brigham Young University

November 22, 2022

Abstract

Thirteen years of precipitation d^2H , $d^{18}O$, and 3H data for three western United States continental interior weather stations, supplemented with 60 years of precipitation data, have been analyzed. The stations are located 1,000 to 2,000 km from four ocean moisture sources. Precipitation was evaluated relative to storm track trajectory, the El Niño-Southern Oscillation Oceanic Niño Index (INO), orography, precipitation amount, air temperature, month, and season. The INO was not found to correlate with precipitation flux or isotopic composition. Tritium deposition was evaluated relative to the 'spring leak', thunderstorms, surface evaporation, storm tracks, and seasons. Local meteoric water lines and the Global Meteoric Water Line were compared. Winter precipitation is isotopically depleted and summer precipitation is isotopically enriched. Factors affecting the stable isotopes include winter cold cloud temperature, summer rain droplet partial evaporation, gradual rain out, and multiple episodes of soil moisture re-evaporation and subsequent re-precipitation.

1 Continental interior storm tracks, tritium deposition, and precipitation isotopes at the Great
2 Basin-Rocky Mountain physiographic provinces transition zone, USA

3 Mayo, A.L.¹, and Tingey, D.G.²

4
5 ¹ Mayo and Associates LC, Phoenix Arizona, alan_mayo@live.com

6 ² Brigham Young University, Provo, Utah USA, dgingey@gmail.com

7

8 Key Points

- 9 • The flux and isotopic composition of Southwestern United States continental interior
10 precipitation are not correlatable with the El Niño-Southern Oscillation Oceanic Niño
11 Index (INO).
- 12 • Tritium deposition is highly variable (2.1 to 29.5 TU) and is influenced by the four storm
13 track trajectories, the ‘spring leak’, thunderstorms, and surface moisture evaporation.
- 14 • Most winter precipitation is isotopically depleted due to cold cloud temperatures and
15 twenty-five percent is seasonally evaporated due to partial rain droplet evaporation.

16

17 **Abstract**

18 Thirteen years of precipitation $\delta^2\text{H}$, $\delta^{18}\text{O}$, and ^3H data for three western United States continental
19 interior weather stations, supplemented with 60 years of precipitation data, have been analyzed.
20 The stations are located 1,000 to 2,000 km from four ocean moisture sources. Precipitation was
21 evaluated relative to storm track trajectory, the El Niño-Southern Oscillation Oceanic Niño Index
22 (INO), orography, precipitation amount, air temperature, month, and season. The INO was not
23 found to correlate with precipitation flux or isotopic composition. Tritium deposition was
24 evaluated relative to the ‘spring leak’, thunderstorms, surface evaporation, storm tracks, and
25 seasons. Local meteoric water lines and the Global Meteoric Water Line were compared.
26 Winter precipitation is isotopically depleted and summer precipitation is isotopically enriched.
27 Factors affecting the stable isotopes include winter cold cloud temperature, summer rain droplet
28 partial evaporation, gradual rain out, and multiple episodes of soil moisture re-evaporation and
29 subsequent re-precipitation.

30 **1 Introduction**

31 The isotopic composition of precipitation is of particular interest to hydrologic and
32 hydrogeologic investigations. Beginning 1953, with the advent of atmospheric thermonuclear
33 testing, the concentration atmospheric bomb ^3H overwhelmed the natural stratospheric ^3H . The
34 long-lasting atmospheric ^3H spike provides a time maker in many water related investigations.
35 Atmospheric bomb ^3H has been exhausted for the past 30 or so years due to the ‘rain out’ effect
36 and more recent precipitation contains natural ^3H concentrations. The short 12.3-year half-life
37 makes ^3H particularly useful for identifying recent groundwater recharge.

38 Stable isotopic molecules are often used to ‘finger print’ water, help sort out phenomena related
39 to precipitation temperature such as climate, elevation and season, to identify evaporated water,
40 and to characterize geothermal groundwater circulation. The study of the stable isotopic ratios
41 $^2\text{H}/^1\text{H}$ and $^{18}\text{O}/^{16}\text{O}$ in natural waters began in the 1930’s (Gilfillan, 1934; Harada, and Titani,
42 1935; Lewis and Cornish, 1933; Tes, 1939) and resumed in earnest after World War II (Craig et
43 al., 1956; Dansgaard, 1953, 1954, 1964; Ehhalt et al., 1963; Epstein, 1956; Epstein and Mayeda,
44 1953; Friedman, 1953; Kobayakawa and Horibe, 1960). In his seminal paper Harmon Craig
45 (Craig, 1961) analyzed 400 samples from worldwide locations of rivers, lakes, and precipitation

46 for the stable isotopic ratios. About 40 percent of the samples were from North America. The
47 purpose of Craig's research was to establish the isotopic relationships of meteoric water. Except
48 for evaporated water in closed basins, the plotted trend of the data is represented by the equation:

$$49 \quad \delta^2\text{H} = 8\delta^{18}\text{O} + 10 \text{‰} \quad (1)$$

50 where $\delta^2\text{H}$ and $\delta^{18}\text{O}$ are the ratios of $^2\text{H}/^1\text{H}$ and $^{18}\text{O}/^{16}\text{O}$, respectively of the sample relative to
51 Standard Mean Ocean Water (SMOW). SMOW is exhausted and the new standard is Vienna
52 Standard Mean Ocean Water (VSMOW). Differences between samples and the standard are
53 small and the differences are reported as permil rather than the more familiar percent. Eq. 1 was
54 originally called the Craig Line and is now known as the widely used Global Meteoric Water
55 Line (GMWL). In Eq. 1 the value 8 is the line slope and +10 is the deuterium intercept on the y
56 axis. The y intercept is also known the deuterium excess. Craig found that the GMWL is
57 consistent with Rayleigh liquid-vapor equilibrium distillation between -10 and 100 °C. Colder
58 precipitation temperatures correspond to more negative isotopic values.

59 In 1964 Dansgaard (1964) analyzed 1,126 stable isotopic results from 84 worldwide
60 International Atomic Energy Agency World Meteorological Organization (IAEA WMO)
61 precipitation network stations. He found that local precipitation data commonly deviate from
62 Rayleigh distillation in that both the line slope and the y intercept can vary greatly. The
63 precipitation network included all continents, except for inland Asia, and numerous oceanic
64 islands. Most of Dansgaard's stations were located near an ocean and each data set included at
65 least one full year of measurements. Since 1964 it has been well documented that the stable
66 isotopic composition of precipitation may be effected by geographic and meteorological factors
67 including latitude, land surface elevation (altitude effect), distance from the coast (rain out
68 effect), season, climate and paleoclimate, surface air temperature, precipitation intensity (amount
69 effect), and storm tracks (Clark and Fritz, 1997; Gat, 2001; Merlivant and Jouzel, 1979;
70 Rozanski et al., 1993; Siegenthaler and Oeschger, 1980; Yurtsever, 1975).

71 Temporal variability in stable isotopic compositions of precipitation have been used 1) to
72 develop local meteoric water lines (Benjamin et al., 2004; Klaus et al., 2015; Yeh, 2014), 2) as
73 proxies for past climate particularly as related to speleothem formation (Cross et al., 2015; Duan

74 et al., 2016; Pape et al., 2010), 3) to evaluate the amount effect (Easto and Dettman, 2016; Hager
75 and Foelsche, 2015), 4) to evaluate interannual temperature changes (Bowen, 2008; Cai and
76 Tian, 2016), and 5) to evaluate seasonal storm tracks (Araguás et al., 1998; Kurita et al., 2014;
77 Vuille and Wermer, 2005). Precipitation stations located in mid-continental settings commonly
78 have seasonal isotopic variations (Gat, 2001; IAEA, 2021). For example, in Vienna, Austria and
79 Ottawa, Canada the average seasonal variations in $\delta^{18}\text{O}$ are as great as 18‰ between winter and
80 summer precipitation. Based on a limited data set Benjamin et al. (2004) found several per mil
81 variability in $\delta^{18}\text{O}$ between winter and summer precipitation events at a single station in the
82 interior of the western United States.

83 Of interest here are the isotopic compositions of precipitation at the Great Basin-Rocky
84 Mountain physiographic provinces transition zone in the interior of the southwestern United
85 States (Fig. 1). The bomb tritium spike in the interior of the southwestern US is well
86 documented in IAEA (2021) data. Benson and Klieforth (1989) measured seasonal stable
87 isotopic variations in southern Nevada, Friedman et al. (1992) and Smith et al. (1992)
88 investigated stable isotopic compositions of precipitation in southern California, and Friedman et
89 al. (2002a) investigated air mass trajectories using 3 years of data (1991-1993) from two
90 locations. Houghton (1979) investigated orographic effects, Friedman et al. (2002b) evaluated
91 spatial stable isotopic trends using seasonal data (1991-1996) from continuous collectors at 41
92 stations, and Benson (2017) investigated precipitation in the southwestern portion of the Great
93 Basin.

94 The purpose of this investigation is to better understand the meteorological and orographic
95 factors that affect the isotopic compositions of precipitation in the interior of the western United
96 States. We have analyzed the isotopic compositions of precipitation from three stations at the
97 transition between in the northeastern Great Basin and the Rocky Mountain physiographic
98 provinces (Fig. 1). The three Utah transition zone locations were selected for study because they
99 potentially receive precipitation from the same storm tracts, yet have very different orographic
100 characteristics. One station, Pilot Valley-Silver Island Range, is located in the Great Basin about
101 190 km west of the Great Basin-Rocky Mountain transition. One station, Lindon, Utah, is
102 located at the transition between the two physiographic provinces at the base of the Wasatch

103 Range. One station is located on the Wasatch Plateau near the top of the Wasatch Range in the
104 Rocky Mountain physiographic province.



105
106 Figure 1 Location of precipitation collection locations in the Great Basin. The Great Basin is a
107 vast region of internal drainage in the western United States is the northern portion of the
108 Basin and Range physiographic province. The Wasatch Range marks the eastern
109 boundary of the Great Basin and separates the Great Basin from the Rocky Mountain
110 physiographic province to the east.

111 2 Data and Methodology

112 Two years of data (2005-2007) were developed for eight cumulative collection stations in Pilot
113 Valley (Fig. 1). The stations were collected monthly and included 133 stable isotope and five ^3H
114 samples. The cumulative collectors were treated with a layer of oil to prevent evaporation. The
115 Pilot Valley stations are located on the western Silver Island Range alluvial fan (windward side).

116 The stations range in elevation from 1,300 m above mean sea level (amsl) on the valley floor to
117 1,650 m amsl on the Silver Island Range alluvial fan, and were located ~3.5 to 5 km west of the
118 range ridge line. Thirteen years (1999 - 2012) of daily precipitation samples were collected at
119 the Lindon station. Analysis included 335 $\delta^2\text{H}$ and $\delta^{18}\text{O}$ and 79 ^3H samples. The Lindon station
120 is located at the base of the Wasatch Range on the very edge of the northeastern Great Basin at
121 an elevation of 1,445 m amsl. The Wasatch Range rises to 3,582 m amsl about 7 km east of the
122 station. One year of bi-weekly snow and rain samples (1999-2000) were collected from the two
123 Wasatch Plateau stations. One station was at 2,682 m amsl and one was at 2,877 m amsl. Snow
124 was collected from the top layer of the snow pack and allowed to thaw in sealed containers and
125 rain was obtained from two oil treated continuous collectors. The plateau is located about 40 km
126 east of the eastern edge of the Great Basin.

127 Laboratory analyses were performed at Brigham Young University facilities. The stable isotopes
128 were analyzed using a Finnegan Delta Plus mass spectrometer and the tritium samples were
129 electrolytically enriched prior to analysis with a 1220 Quantulus ultra low-level liquid
130 scintillation spectrometer. $\delta^{18}\text{O}$ and $\delta^2\text{H}$ measurements are ± 0.3 and 1.0 ‰, respectively, and
131 the ^3H minimum detection limit (MDL) is 0.3 TU.

132 Storm tracks for each Lindon station sampling date were determined using the National Oceanic
133 and Atmospheric Administration (NOAA) program HYSPLIT (NOAA, 2021). Stable isotopic
134 data were statically compared to the GMWL by creating a synthetic GMWL data set for the local
135 data. The synthetic GMWL data was developed by calculating a $\delta^2\text{H}$ for each laboratory $\delta^{18}\text{O}$
136 value using Eq. 1. The synthetic $\delta^2\text{H}$ data and the laboratory data for each sample were then
137 statically compared at the 95 percent confidence level.

138 Salt Lake City station ^3H data for 1963-1984 was obtained from the IAEA Global Network of
139 Isotopes in Precipitation (GNIP) electronic data base (IAEA, 2021). The 230 Salt Lake City
140 samples were from bi-weekly sampled continuous collectors. The Salt Lake station is located 50
141 km north of the Lindon station and occupies the same orographic position at the base of the
142 Wasatch Range as the Lindon station. Precipitation amount data from the Wendover, Pleasant
143 Grove, and Fairview weather stations (WRCC, 2021) were analyzed as surrogates for long-term
144 Pilot Valley, Lindon, and Wasatch Plateau station data, respectively. The surrogate stations are

145 located within a few km of the study area stations and occupy similar physiographic and
146 orographic positions.

147 The tritium and stable isotopic data for Pilot Valley, Lindon and Wasatch Range stations has
148 been reported to the IAEA for inclusion in the GNIP data base and are available online.

149 Pilot Valley, Lindon and Wasatch Plateau stable isotopic and tritium data developed as part of
150 this research, and Salt Lake City tritium data are archived with the IAEA Global Network of
151 Isotopes in Precipitation (GNIP) electronic data base (IAEA, 2021). Wendover, Pleasant Grove
152 and Fairview, Utah precipitation data are available from the (WRCC, 2021).

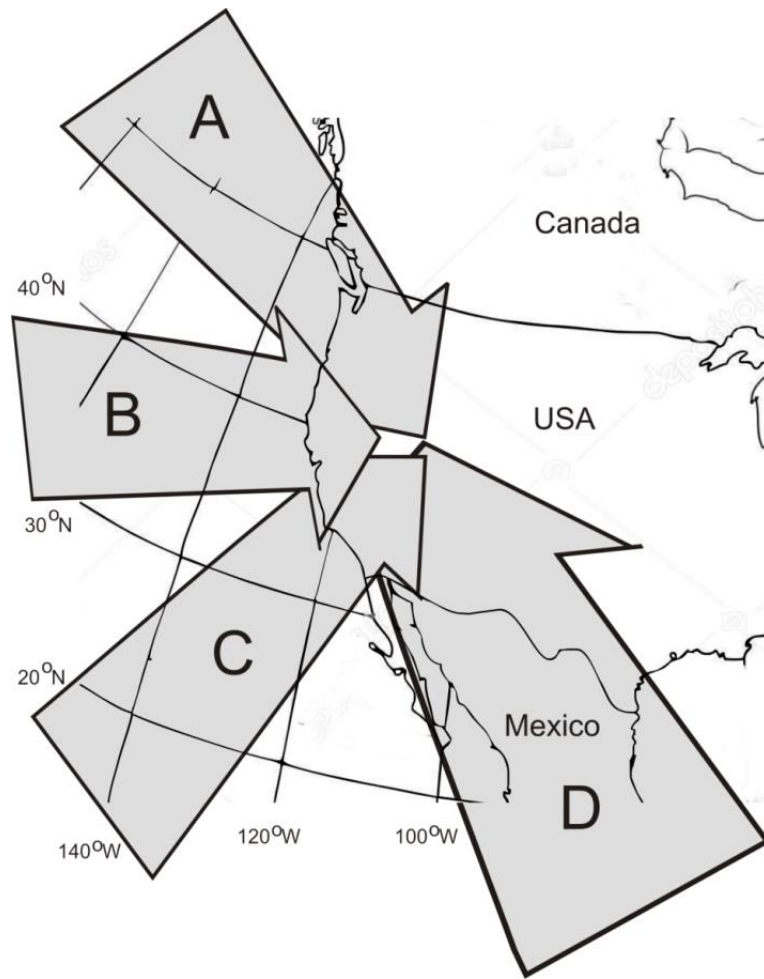
153 **3 Great Basin Orography, Storm Tracks, and Climate**

154 The Great Basin, a 541,700 km² endorheic region, occupies the northern portion of the Basin and
155 Range physiographic province (Fig. 1). The Basin and Range is characterized by extension fault
156 block mountain ranges and valleys. The Great Basin contains more than 100 valleys, bounded
157 by more than 130 named north to northeast trending high mountain ranges, mountains, and hills
158 that have been described as aligned like a march of caterpillars. The mountain ranges are 95 to
159 190 km long and 5 to 24 km wide, and the valleys are commonly wider. The Silver Island
160 Range, an easternmost Great Basin mountain range, rises to 2,260 m amsl and is 960 m above
161 the adjacent Pilot Valley basin. The Wasatch Range marks the transition between the Great
162 Basin to the west and the central Rock Mountain physiographic province to the east. The range
163 rises as much as 2,500 m above the valley floors to the west. The range runs about 260 km from
164 the border with Idaho in the north to south-central Utah in the south. Although the Wasatch
165 Range is part of the Rocky Mountain physiographic province, the range drains into and is the
166 largest Great Basin watershed. The Wasatch Plateau, located in the central Wasatch Range, has
167 an average elevation of 2,690 m amsl.

168 Storms reaching the northeastern Great Basin-Rocky Mountain transition zone are carried along
169 four different air mass trajectories (Houghton, 1969; Friedman et al., 2002a). The trajectories
170 are: 1) cold polar air originating in the Arctic, 2) the western flow of cool North Pacific Ocean air,
171 3) the northwestern flow tropical Pacific Ocean air, sometimes known as the Pineapple Express,
172 and 4) the northern flow of tropical Gulf of California-Gulf of Mexico air (Fig. 2). The

173 air masses originate at ocean sources 1,000 to 2,000 km from the transition zone. Examples of
174 individual storm tracks are shown on Fig. 3. Arctic air peaks in the winter and is not a factor in
175 the summer (Fig. 4). North Pacific air peaks in the winter and early spring, and tropical Pacific,
176 and Gulf of California-Gulf of Mexico air peaks in the summer. Gulf of California-Gulf of
177 Mexico air is often associated with the North American Monsoon (NAM) which provides warm
178 moist air that provides the moisture for most mid-summer to early fall thunderstorms. The
179 influence of the Great Basin on air masses varies greatly by trajectory. During the study period
180 the percentage of storm carrying air mass trajectories that cross the Great Basin before reaching
181 the Lindon station vary by source area: Arctic 16 percent, North Pacific 87 percent, tropical
182 Pacific 44 percent, and Gulf of California-Gulf of Mexico 7 percent. It was not possible to make
183 similar calculations for the Pilot Valley and Wasatch stations, because the precipitation at these
184 stations was collected using continuous collectors that were not monitored daily. It is likely that
185 the Wasatch Plateau station has similar percentages of storm air mass trajectories crossing the
186 Great Basin as the Lindon station. Almost all Pilot Valley storms must cross some or all of the
187 Great Basin.

188 Air masses traversing the Great Basin rapidly undergo numerous adiabatic cooling and heating
189 cycles as the air rises and falls when crossing the relatively narrow mountain ranges. Frequently
190 storms traverse the Great Basin in 36 hours or less (Fig. 3). Assuming average winter and
191 summer Great Basin adiabatic lapse rates of 3.8 and 6.5 °C/km (Patrick, 2014; Dobrowski et al.,
192 2009) and the average mountain block relief is 1 km, the near surface air would cool and heat
193 several °C each time it crosses a mountain range. The heating and cooling results in increased
194 precipitation at high mountain block elevations and more arid conditions in the valley floors.
195 Average annual valley floor precipitation can be as small as 15 cm and mountain peak
196 precipitation can be as great as 70 cm (Jeton et al., 2005; McEvoy et al., 2014). The net effect of
197 this cooling and heating on the isolated mountain ranges are twofold: 1) the ranges are small,
198 snow-pack dominated water sheds that are subject to interannual and decadal precipitation
199 variability, and 2) precipitation falling on the ranges and valleys are subject to the isotopic
200 elevation and rain out effects. Air masses that do not cross the Great Basin also undergo
201 adiabatic changes but less frequently.



202

203 Figure 2 Storm tracks that provide moisture to the northeastern portion of the Great Basin: A)
 204 polar Arctic air, B) cool, north Pacific Ocean air, C) tropical Pacific ocean air, and D)
 205 summer monsoon Gulf of California and Gulf of Mexico air. Continental summer
 206 thunderstorm air usually tracts from the west across the Great Basin.

207

208

209

210

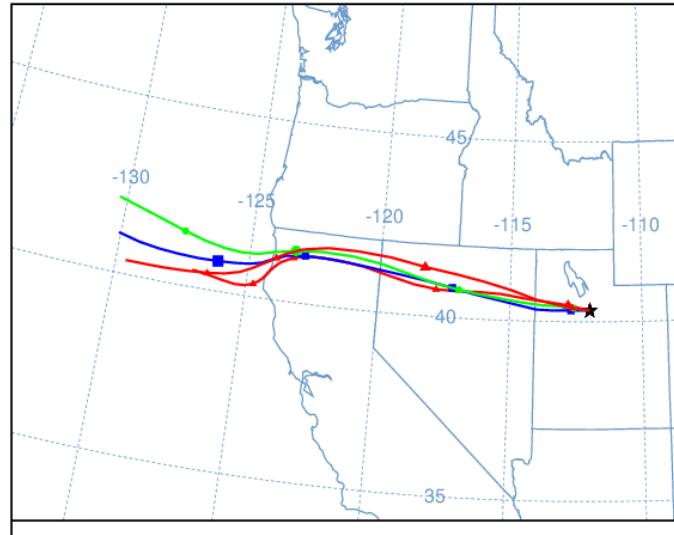
211

212

213

214

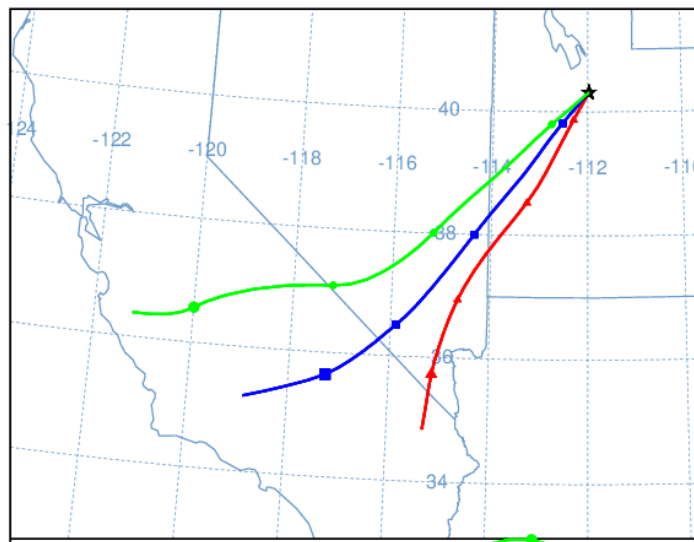
a) North Pacific storm track (November 30-December 1, 2001)



215

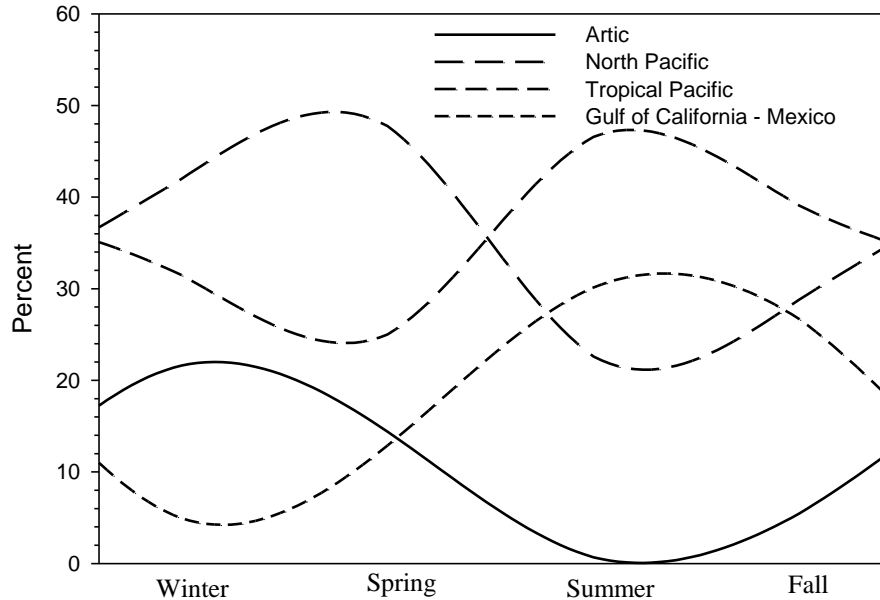
216

b) Tropical Pacific Storm Track (December 31-January 1, 2005)



217

218 Fig. 3 Examples of NOAA HYSPLIT calculated 24 hour storm tracks reaching the Lindon
219 station. North Pacific storms cross the Great Basin about 87 percent of the time and only
220 about 44 percent of tropical Pacific storms cross the southern portion of the Great Basin.
221 The symbols on the air mass trajectories represent 6-hour intervals.



222

223 Fig. 4 Storm tracks associated with isotopic sampling events.

224 The Wasatch Range forms a physiographic barrier that influences and deflects storm tracks from
 225 the north, west, and south. Once the air mass ascends the Wasatch Range the air remains cool
 226 for an extended period of time as it passes over the relatively high and wide mountains and
 227 valleys of the range. Most tropical Pacific and Gulf of California-Gulf of Mexico air masses first
 228 reach the southern end of the Wasatch Range and then are funneled northward along the western
 229 side of the range before reaching the Lindon Station at the north end of the range. Tropical
 230 Pacific storms that cross the Great basin only skirt the southernmost portion of the basin,
 231 whereas North Pacific air masses typically cross entire Great Basin.

232 In addition to the storm track trajectories Great Basin and transition zone precipitation can be
 233 affected by the complex interaction of the El Niño-Southern Oscillation (ENSO), the Pacific
 234 Decadal Oscillation (PDO), and other Pacific Ocean atmospheric and ocean sea surface
 235 temperature (SST) trends (Mantua and Hare, 2002; Smith et al., 2015). ENSO impacts global
 236 atmospheric circulation including temperature and precipitation and has patterns that persist for 6
 237 to 18 months. ENSO has three phases El Niño, Neutral, and La Niña. The severity of the phases
 238 is measured by NOAA using the Oceanic Niño Index (ONI). ONI is the 3-month running

239 average change in SST at the equator between 120° W and 170° W. El Niño occurs when the
240 tropical Pacific Ocean is warmer and the index is +0.5 °C or higher than the 30-year average. La
241 Niña occurs when tropical Pacific Ocean is cooler and the index is -0.5 °C or lower than average.
242 Neutral is when the index is between +0.5 and -0.5. El Niño causes the Pacific jet stream to
243 move south and La Niña cause the jet stream to move north. Unlike ENSO, PDO events persist
244 for 20-30 years and mostly affect the North Pacific and adjacent North America. PDO is a
245 measure of decadal trends in North Pacific Ocean SST.

246 The northern Great Basin is located at the ENSO forced winter weather transition boundary. The
247 boundary is also known as the ENSO dipole or North American dipole. South of the transition a
248 winter El Niño typically results in wetter conditions in the southwestern US and warmer and
249 dryer conditions than usual north of the transition (Wang et al., 2012). La Niña is the opposite.
250 Coupling of the ENSO dipole with the Pacific Decadal Oscillation (PDO; Mantura and Hare,
251 2002) other Pacific Ocean atmospheric and SST oscillations can shift the North American dipole
252 to the north and to the south, thus greatly effecting northern Great Basin and transition zone
253 precipitation rates, precipitation sources, and air temperatures (Brown, 2011; Smith et al., 2015;
254 Wise, 2010). The net effect of this shift is wet and dry cycles of varying durations.

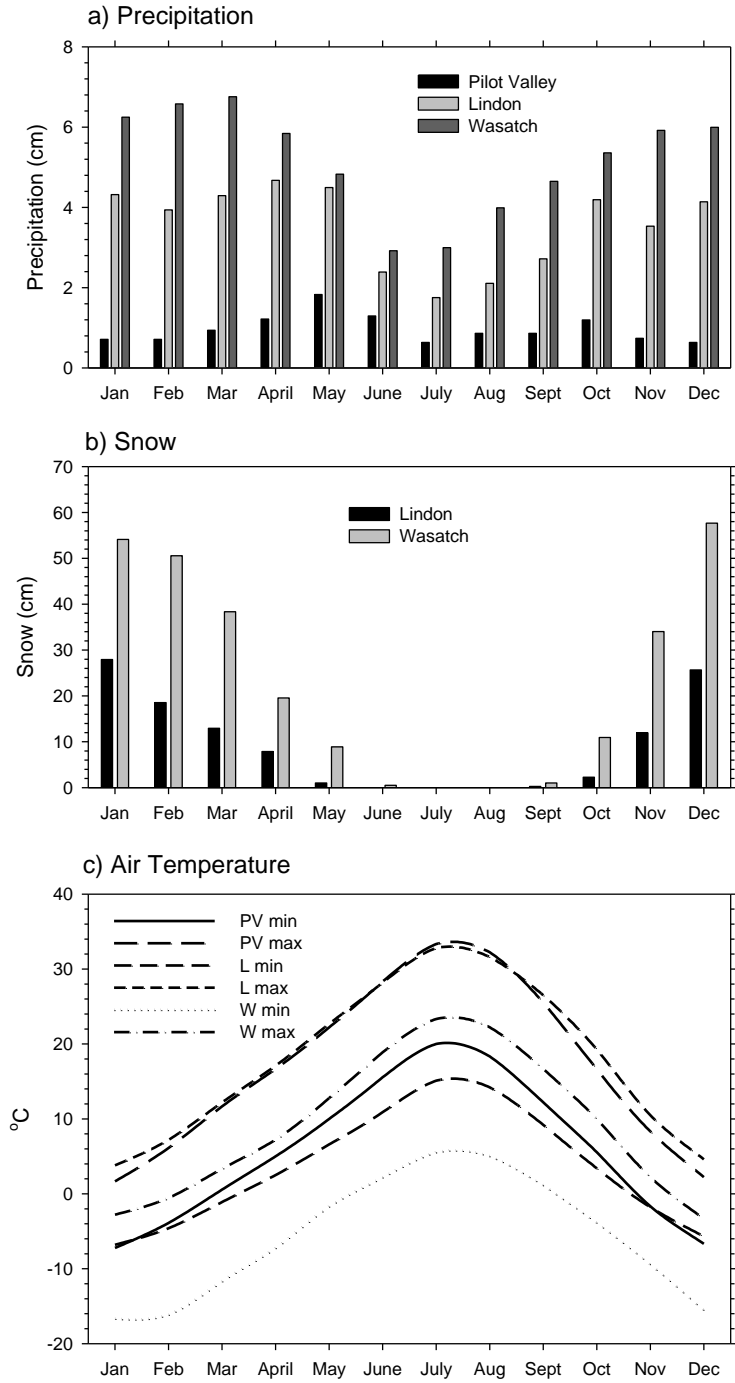
255 **4 Analysis and Discussion**

256 **4.1 Precipitation**

257 The climate at the three sampling stations progresses from semi-arid desert in Pilot Valley to
258 humid continental (Step) in the Wasatch Plateau. At the Lindon and Wasatch Plateau stations
259 winter is wet and cold, spring and fall are wet with variable temperatures, and summer is
260 generally warm and dryer (Fig. 5). Much of the precipitation at the Wasatch station accumulates
261 as snowfall. Snow accumulation is variable at the Lindon station and is infrequent at the Pilot
262 Valley station. Pilot Valley precipitation usually peaks in the spring and early summer.

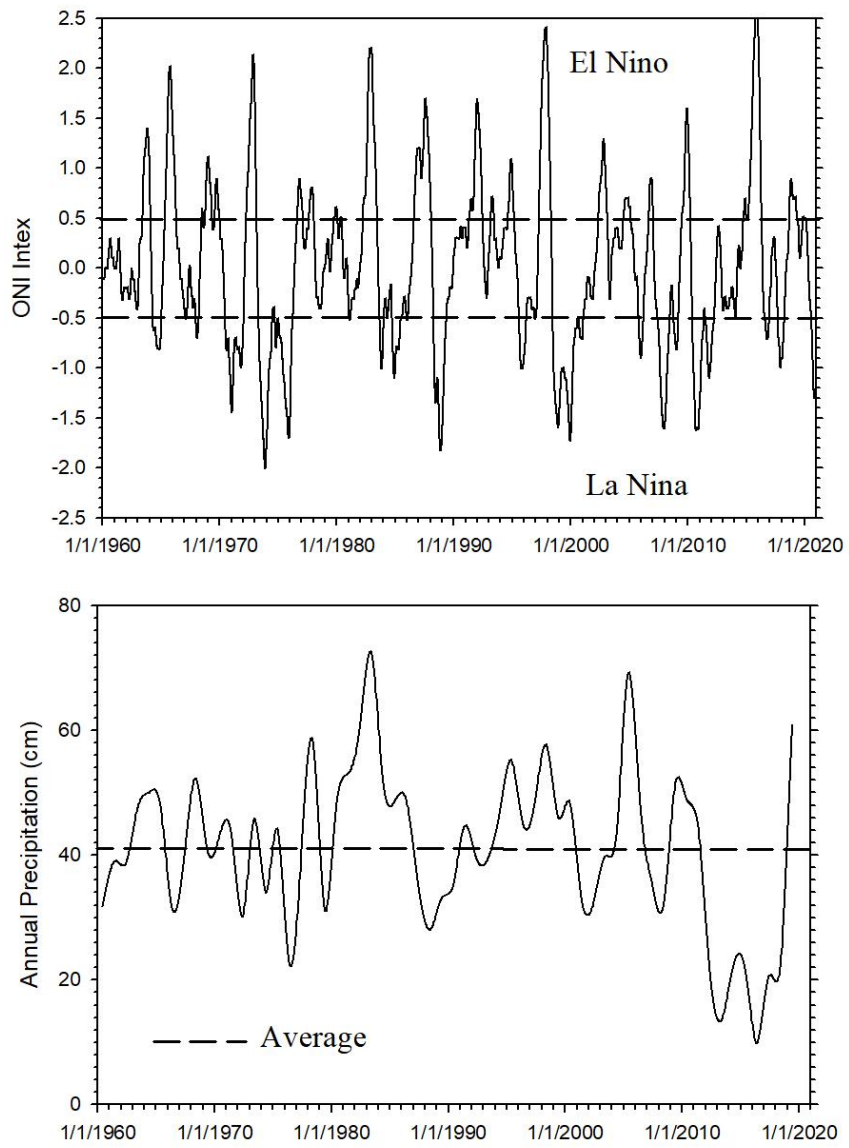
263 Based on an analysis of 60 years of Pleasant Grove monthly and annual precipitation data (1960-
264 2020), there is no correlation between ENSO conditions and the average monthly and average
265 storm total precipitation (Figs. 6 and 7). ONI index values were statically compared to Pleasant
266 Grove monthly, 3-month running averages (732 events), and cumulative storm event totals

267 (1,108 events). The R^2 values of the correlation of the ONI vs. Pleasant Grove data range from
268 0.001 to 0.00003. An R^2 of 0.001 means that only 0.1 percent of the precipitation variability can
269 be explained by the ONI index. There is also no correlation between long-term Wendover, UT
270 (1960-2016), and Fairview, UT (1975-2010) precipitation data with ONI data. The R^2 values for
271 the Wendover and Fairview data are 0.012 and 0.00012 respectively. Except for the Pleasant
272 Grove February El Niño vs. neutral and vs. La Niña, and the December El Niño vs. La Niña
273 storm event averages, there are no statistical differences between the ONI and either the monthly
274 or storm event total precipitation amounts. The absence of correlation between the long-term
275 precipitation data and ONI index means that the index is not a reliable predictor of transition
276 zone precipitation or for use as a standalone tool for assessing transition zone precipitation
277 isotopic data. Smith et al. (2015) simulated the effects of ENSO and PDO on Great Basin
278 precipitation and found that ENSO over predicted and PDO under predicted precipitation. The
279 lack of correlation between the ONI index and transition zone precipitation may be related to
280 north and south migration of the North American Dipole.



281

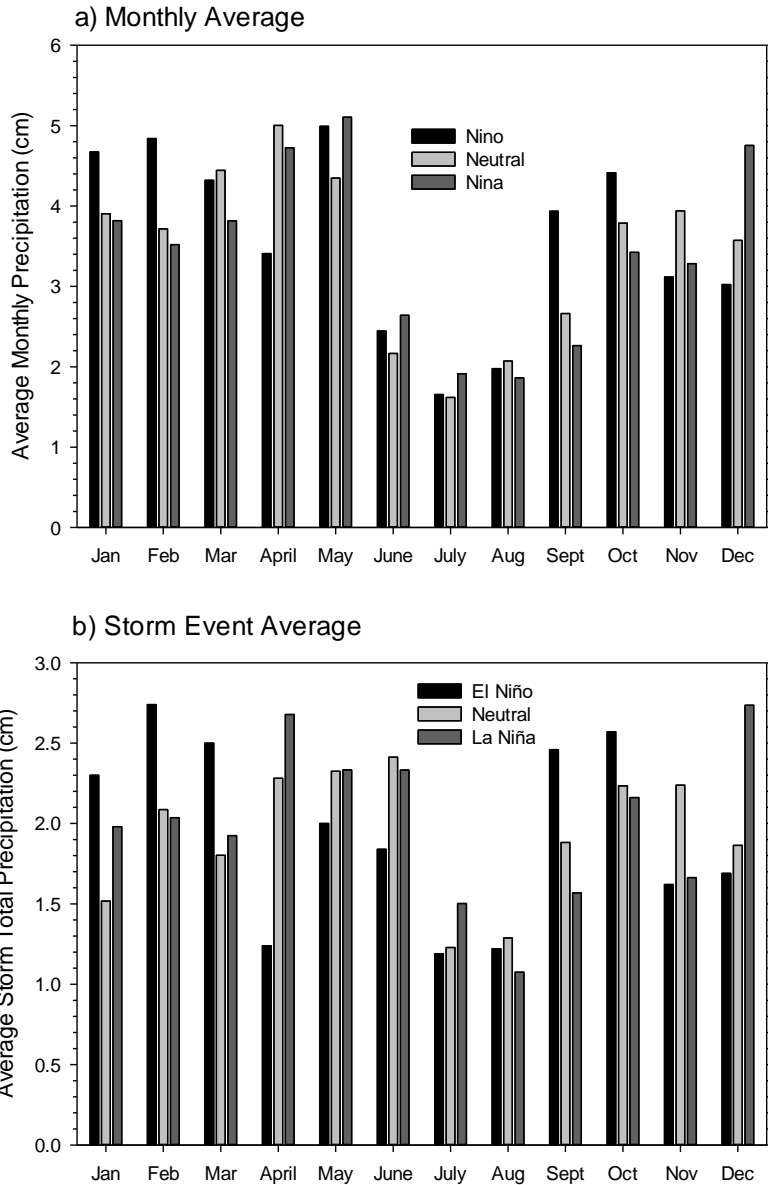
282 Fig. 5 Climate summary for Pilot Valley (PV), Lindon (L) and Wasatch Range (W) sampling
 283 stations. Data are 40 year averages.



284

285 Fig 6 Comparison of ONI index and Pleasant Grove average annual precipitation.

286



287

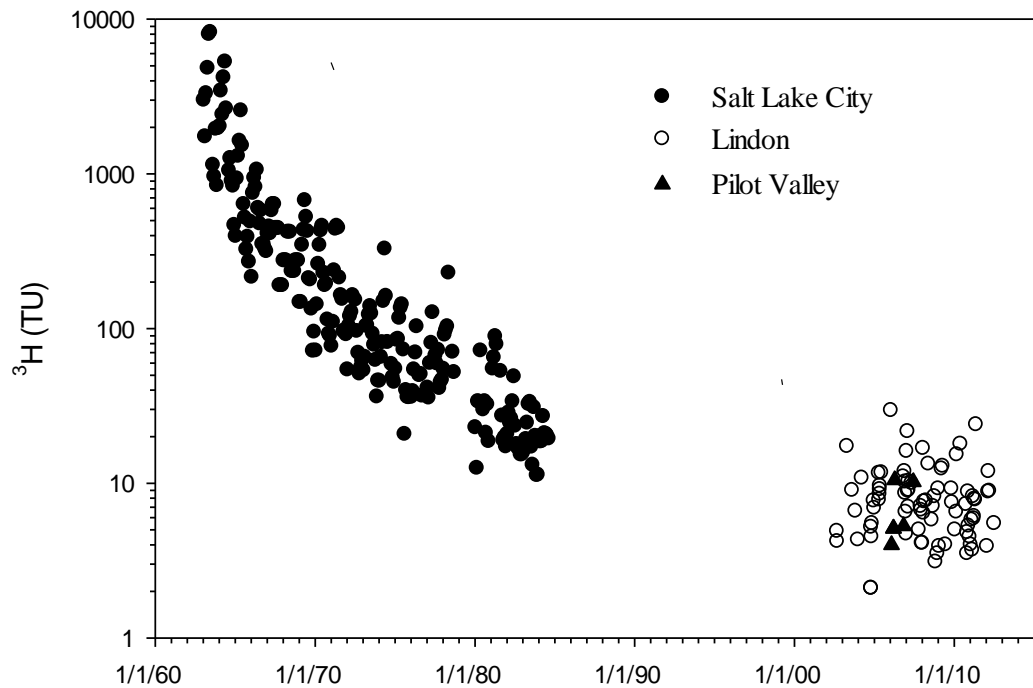
288 Fig. 7 Average Pleasant Grove station monthly total and storm event precipitation between 1960
 289 and 2020.

290 **4.2 Tritium Deposition**

291 Transition zone tritium deposition has been measured at both the Salt Lake City and Lindon
 292 stations (Fig. 8). The Salt Lake City data reflect the rain out effect after the cessation of
 293 atmospheric thermonuclear testing in 1963. In 1963 individual storm events contained as much
 294 as 10,000 TU. By 1994, at that end of the Salt Lake City sampling, the atmosphere contained
 295 near natural atmospheric ³H concentrations. The Lindon data represent natural atmospheric ³H

296 deposition. The average and median ^3H concentrations of the Lindon precipitation are 8.5 and
297 7.6 TU, respectively, and the minimum and maximum concentrations are 2.1 and 29.5 TU. The
298 standard deviation is 4.8 TU. The limited number of Pilot Valley samples had similar
299 concentrations as the bulk of the Lindon samples. The ^3H concentrations in Lindon and Pilot
300 Valley precipitation varied greatly between 2002 and 2012. There is no correlation between
301 Lindon ^3H concentrations and precipitation amount or temperature, but there are statistical
302 differences between the spring (March-May) and fall (September-November) data (Fig 9a), and
303 between the Gulf of California-Gulf of Mexico storm tracks with the North Pacific and Arctic
304 storm tracks (Fig 9b). Factors that influence the concentration variability in natural tritium
305 deposition and the statistical differences are discussed below.

306 Natural tritium is produced in the lower stratosphere and upper troposphere by the bombardment
307 of cosmic rays. This tritium is rapidly removed as atmospheric water vapor only has a residence
308 time of 10-30 days. Coastal precipitation typically has low tritium concentrations due to the
309 exchange of atmospheric water vapor with the low tritium concentrations in ocean surface
310 water (Schell et al., 1970; Suess, 1970). When storm systems move inland (continental
311 effect) troposphere tritium concentrations increase by varying amounts as tritium deposition is
312 affected by the timing and flux of stratosphere-troposphere exchange, and by near land surface
313 processes. Processes that increase tropospheric tritium concentrations in the Great Basin-
314 Wasatch Range area include the so called 'spring leak', thunderstorms, and near surface
315 evaporation. The spring leak occurs in the spring time when the tropopause breaks down
316 between 30°N and 60°N and permits the mixing of troposphere air with tritium rich stratosphere
317 air (Michel et al., 2018). Elevated tritium deposition is also associated with summer
318 thunderstorm thunderheads that penetrate the troposphere and bring down precipitation with
319 elevated ^3H concentrations. Evaporation and atmospheric exchange of inland surface water and
320 saturated soil with elevated tritium can also increase inland tritium deposition. Evaporation
321 peaks in the spring and summer. The consequence of these processes combined with the
322 variability in storm track trajectories results in the wide range of ^3H concentrations in modern
323 precipitation. For example, spring and summer storm tracks crossing the Great Basin are subject
324 to considerable precipitation and re-evaporation, and summer thunderstorms commonly involve
325 the NAM.



326

327 Fig. 8 Tritium concentrations in transition zone precipitation.

328 **4.3 Stable Isotopes**

329 The Lindon $\delta^{18}\text{O}$ data ranges from 3.36 to -28.18 ‰ with average and median values of -14.25
 330 and -14.16 ‰, respectively. The $\delta^2\text{H}$ data ranges from 7 to -215.4 ‰ with average and median
 331 values of -107.74 and -107.0 ‰, respectively. The stable isotopic data for all three stations have
 332 been plotted relative to the GMWL (Fig. 10). Local meteoric water lines (LMWL) calculated for
 333 each data set and for the cumulative data are:

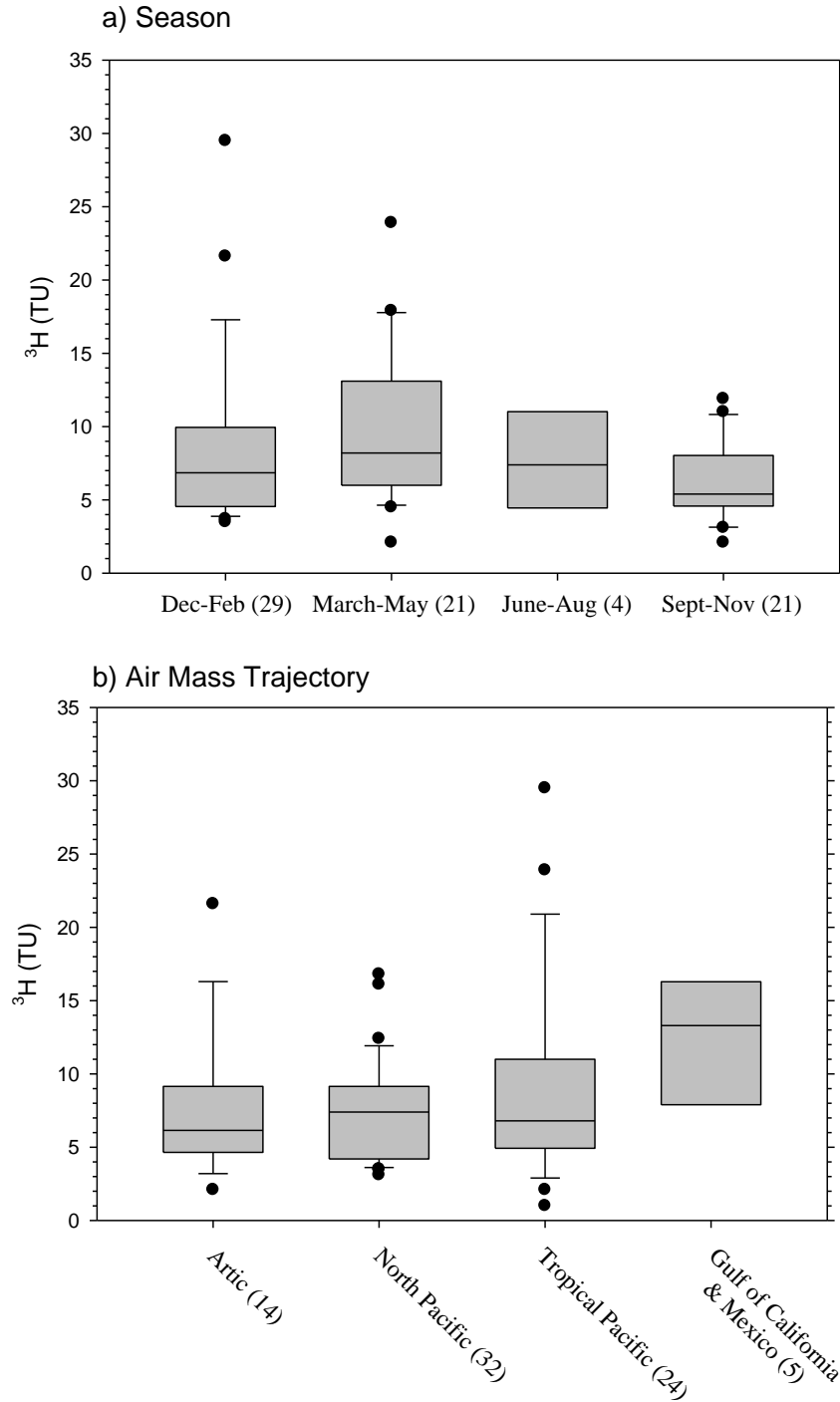
334 Pilot Valley $\delta^2\text{H} = 7.0 \delta^{18}\text{O} - 14 \text{ ‰}$ (2)

335 Lindon $\delta^2\text{H} = 7.2 \delta^{18}\text{O} - 5.1 \text{ ‰}$ (3)

336 Wasatch Plateau $\delta^2\text{H} = 8.7 \delta^{18}\text{O} + 27.7 \text{ ‰}$ (4)

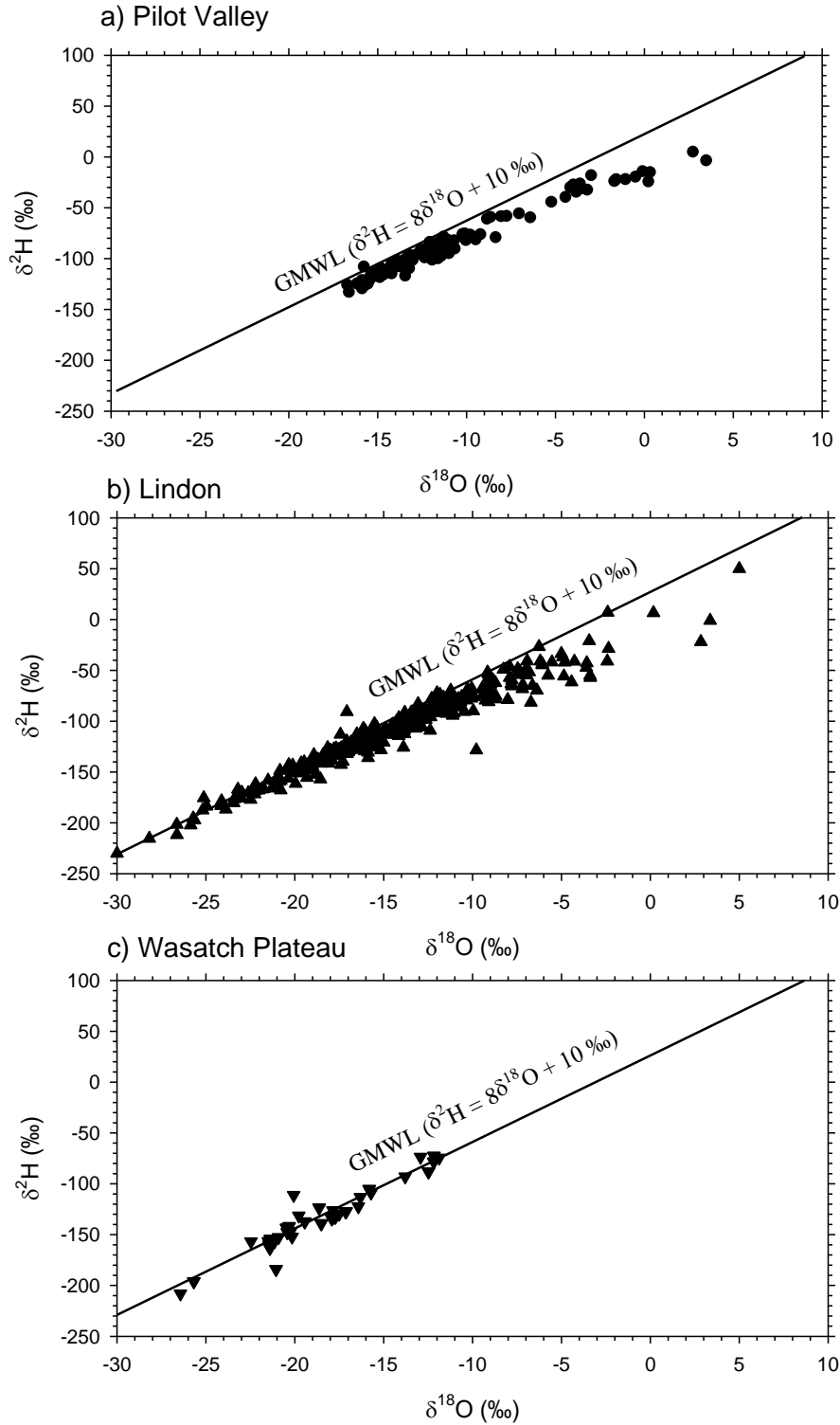
337 Cumulative data $\delta^2\text{H} = 7.0 \delta^{18}\text{O} - 8.3 \text{ ‰}$ (5)

338



339

340 Fig. 9 Box plots of ^3H concentrations in Lindon precipitation organized by season (a) and storm
 341 track trajectory (b). The numerical values associated with the seasons and storm tracks
 342 are the number of samples. The line in the box is the median value (Q2 or 50th
 343 percentile), the top and bottom of the box are the 75th percentile (Q3) and the 25th
 344 percentile (Q1), and the bottom and top whiskers are $Q1 - 1.5 \cdot \text{IQR}$ and $Q3 + 1.5 \cdot \text{IQR}$,
 345 respectively, where IQR is the 25th to 75th percentile. Outliers are shown as filled circles.



346

347 Fig. 10 Pilot Valley (a), Lindon (b) and Wasatch Plateau (c) precipitation stable isotopic
 348 compositions plotted relative to the GMWL.

349

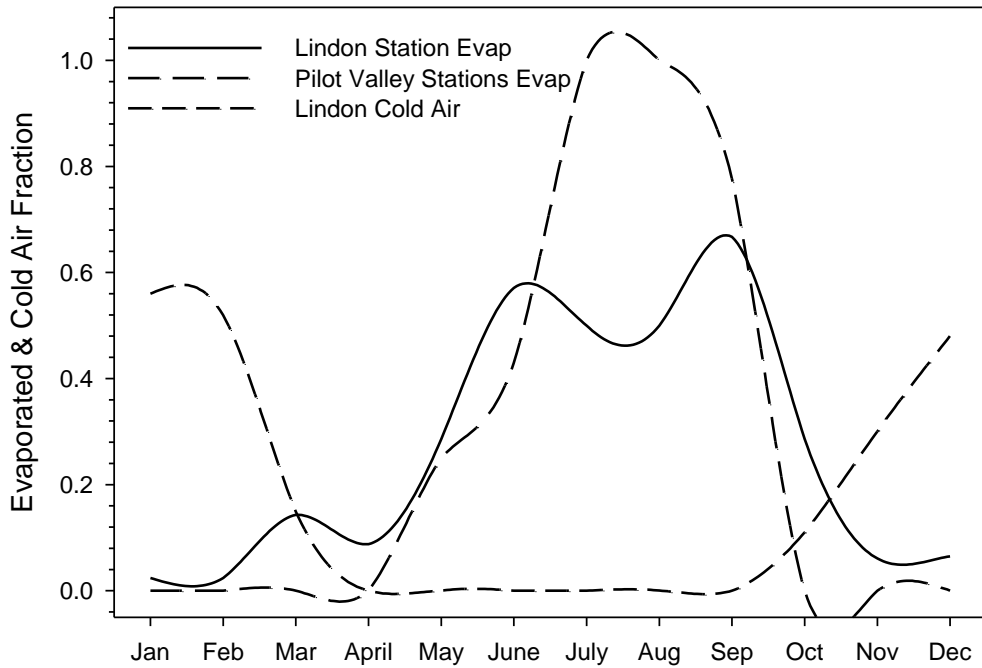
350 Although the LMWL's differ from the GMWL, there are no statically significant differences
351 between the Lindon and Wasatch Plateau data relative to the GMWL. The p values for the
352 GMWL vs. Lindon and Wasatch data are 0.2923 and 0.4348, respectively. What this means is
353 that the GMWL is a reasonable surrogate for Wasatch Front and Wasatch Range precipitation.

354 Pilot Valley precipitation differs significantly from the GMWL with a p value of 0.0231. Much
355 of the Pilot Valley data plots subparallel to the GMWL, and the data with values > -11 ‰ in ($> -$
356 78 ‰ $\delta^2\text{H}$) plot along a possible evaporation trajectory (Fig 10a). A similar apparent
357 evaporation trend occurs in the Lindon data (Fig. 10b). The percentage of Lindon and Pilot
358 Valley precipitation that has been subjected to partial evaporation (i.e., $\delta^{18}\text{O} > -11$ ‰) are 24
359 and 30 percent, respectively. Partial evaporation of precipitation begins in late spring and
360 continues through early fall (Fig. 11). By summer when the air is warmer, thunderstorms are
361 common, and the NAM begins about half of the Lindon precipitation and all of the Pilot Valley
362 precipitation has undergone some evaporation. The evaporative signatures are attributed to the
363 partial evaporation of rain droplets accompany the free fall of rain. In the summer and early fall
364 it is not uncommon for rain to completely evaporate before reaching the ground (virga effect).
365 Partial evaporation in the Great Basin has been reported by Friedman et al. (2002b). The
366 subparallel plotting of the Pilot Valley data is attributed to the combined factors of isotopic
367 fractionation accompanying rain out and the contributions from multiple episodes of re-
368 evaporation and subsequent re-precipitation of soil moisture as storms cross the Great Basin.

369 In addition to the partial evaporation several trends are apparent when the Lindon data are
370 plotted relative to month, season, and storm track (Fig. 12). Median $\delta^2\text{H}$ values are most
371 negative in the winter (December - February) and early spring (March) and become less negative
372 in the late spring through fall (April-October; Fig. 12a). Except for winter vs. spring all of the
373 seasonal data are statistically different from each other. The spring data are skewed toward more
374 negative values (Fig. 12b). When March is not included with April and May the spring time data
375 is statistically different than the winter data. Storm track median $\delta^2\text{H}$ precipitation values
376 become heavier from the Arctic to the Gulf of California-Gulf of Mexico (Fig.12c). The Gulf of
377 California-Gulf of Mexico trajectory precipitation data are statically heavier than all other air
378 trajectory data. The less negative values caused by rain droplet partial evaporation is the result
379 of warm, late spring and summer tropical Pacific and Gulf of California-Gulf of Mexico air (Fig.

380 4). About 50 percent of Lindon winter precipitation is associated with very cold cloud
381 conditions (i.e., $\delta^{18}\text{O} < \sim -17\text{‰}$). Between April and October, when Arctic and north Pacific air
382 trajectory storm are less frequent, all of the Lindon precipitation $\delta^{18}\text{O}$ is $> -17\text{‰}$.

383

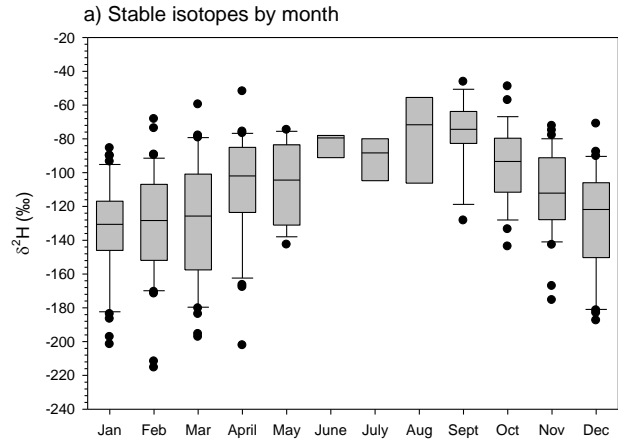


384

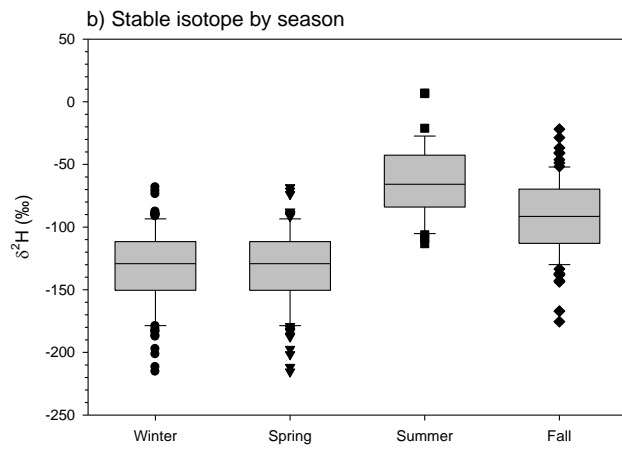
385 Fig.11 Fraction of precipitation that is partially evaporated and that formed during very cold
386 cloud conditions. Evaporation = $\delta^{18}\text{O} > -11\text{‰}$ and cold cloud = $\delta^{18}\text{O} < -17\text{‰}$.

387

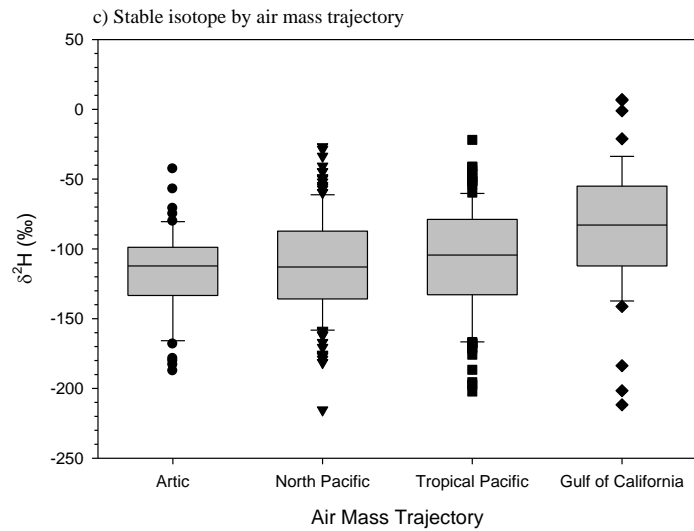
388



389



390



391 Fig. 12 Box plots of Lindon $\delta^2\text{H}$ data organized by month (a), season (b) and air mass trajectory
392 (c).

393

394 **5 Conclusions**

395 The Wasatch Range forms a physiographic and orographic barrier that has a profound impact on
396 the oceanic air mass trajectories that cross the interior of the southwestern United States. The
397 southeast flowing cold Artic air, west flowing cool North Pacific Ocean air, and northeast
398 flowing tropical Pacific Ocean air originate in the Pacific Ocean 1,000 to 1,500 km from the
399 Wasatch Range. North flowing Gulf of California-Gulf of Mexico air originates in the Gulf of
400 California and Gulf of Mexico 1,000 to 2,000 km away. The percentage of storm carrying air
401 mass that reaching the base of the Wasatch Range vary by source area and season. When the air
402 masses reach the Wasatch Range the north and south flowing air is partially funneled along the
403 range front.

404 In the study area the Oceanic Niño Index (ONI) is not a reliable predictor of precipitation flux or
405 for use as a standalone tool for assessing precipitation isotopic composition. The lack of
406 correlation between the ONI index with transition zone precipitation or isotopic composition is
407 likely influenced by the north-south migration of the ENSO Dipole (aka North American
408 Dipole). Coupling of the ENSO Dipole with other Pacific Ocean atmospheric and SST
409 oscillations shifts the ENSP Dipole north and south. The varying durations of wet and dry cycle
410 are like related to this migration.

411 The flow of moisture from the ocean sources to the continental interior results in tritium
412 enrichment and stable isotopic depletion. Modern tritium deposition averages 8.5 TU and ranges
413 between 2.1 and 29.5TU. Average tritium concentrations are greater in the spring time and from
414 storms associated with tropical Pacific and Gulf of California-Gulf of Mexico air. Elevated
415 tritium deposition is associated with the so called 'spring leak', thunderstorms, and land surface
416 evaporation. These processes combined with the variability in storm track trajectories results in
417 modern precipitation having a wide range of tritium concentrations.

418 Local meteoric water lines (LMWL) for the Lindon station and the cumulative LMWL are:

$$419 \text{ Lindon } \delta^2\text{H} = 7.2 \delta^{18}\text{O} - 5.1\%$$

420 Cumulative data $\delta^2\text{H} = 7.0$ $\delta^{18}\text{O} - 8.3\text{‰}$

421 Although the LMWL's differ from the GMWL, there are no statically significant differences
422 between the Lindon and cumulative LMWL's and the GMWL, thus the GMWL can be used as a
423 reference for surface and groundwater investigations. Most winter precipitation is isotopically
424 depleted relative to precipitation falling the rest of the year. The depleted isotopic signatures are
425 attributed to the cold, winter cloud temperatures. About 25 to 30 percent of the precipitation is
426 seasonally evaporated. The evaporative signatures are due to the partial evaporation of rain
427 droplets accompany the free fall of rain. Great Basin precipitation plots sub-parallel to the
428 GMWL. The subparallel plotting is attributed to the combined factors of isotopic fractionation
429 accompanying gradual rain out and the multiple episodes of re-evaporation and subsequent re-
430 precipitation of soil moisture as storms cross the numerous Great Basin mountain ranges.

431 **6 Acknowledgments**

432 This research was supported by the Brigham Young University Laboratory of Isotope
433 Hydrogeology.

434 **7 References Cited**

- 435 Araguás, L., Froehlich, K. & Rozanski, K. (1998). Stable isotope composition of precipitation
436 over southeast Asia. *J. Geophys. Res.* 103 (D22), 28721–28742.
- 437 Benson, L. (2017). Great Basin surface water and precipitation isotopic data.
438 <https://digitalcommons.unl.edu/cgi/viewcontent.cgi?article=1001&context=usgsdata>,
439 accessed 2/12/21
- 440 Benson, L. & Klieforth, H. (1989). Stable isotopes in precipitation and ground-water in the
441 Yucca Mountain region, southern Nevada: Paleoclimatic implications, in *Aspects of*
442 *Climate Variability in the Pacific and Western Americas. Geophys. Monogr. Ser., 55*, 41-
443 59.
- 444 Benjamin, L., Knobel, L.L., Hall, L.F., Cecil, L.D. & Green J.R. (2004). Development of a local
445 meteoric water line for southeastern Idaho, western Wyoming, and south-central
446 Montana. *U.S. Geol. Surv. Sci. Inv. Rpt.* 2004-5126, 17 p.
- 447 Bowen, G.J. (2008). Spatial analysis of the intra-annual variation of precipitation isotope ratios
448 and its climatological corollaries. *J. Geophys. Res.*, 113, D05113.
449 doi:10.1029/2007JD009295

- 450 Brown, D. P. (2011). Winter circulation anomalies in the western United States associated with
451 antecedent and decadal ENSO variability. *Earth Interact.* 15. doi:10.1175/2010EI334.1.
- 452 Cai, Z., & Tian, L. (2016). Atmospheric controls on seasonal and interannual variations in
453 precipitation isotope in East Asian Monsoon region: Atmospheric controls on seasonal
454 and interannual variations in the precipitation. *Am. Meteor. Soc.*
455 <http://dx.doi.org/10.1175/JCLI-D-15-0363.1>
- 456 Clark ID, Fritz P. (1997). *Environmental Isotopes in Hydrogeology*. CRC press: Boca Raton.
- 457 Craig, H., (1961). Isotopic variations in meteoric waters. *Sci.*, 133, 1702-1703.
- 458 Craig, H., Boato, G. & White, D.E. (1956). Isotopic geochemistry of thermal waters: *Nat. Acad.*
459 *Sci. Nucl. Sci. Ser. Rep* 19, 29-36.
- 460 Cross, M., McGee, D., Broecker, W. S., Quade, J., Shakun, J. D., Cheng, H., Lu, Y. & Edwards,
461 R. L. (2015). Great Basin hydrology, paleoclimate, and connections with the North
462 Atlantic: A speleothem stable isotope and trace element record from Lehman Caves, NV.
463 *Quat. Sci. Rev.* 127, 186-198. doi.org/10.1016/j.quascirev.2015.06.016
- 464 Danasgaard, W. (1953). The abundance of O18 in atmospheric water and water vapour. *Tellus*,
465 5, 461-469.
- 466 Danasgaard, W. (1954). The abundance of O18 in fresh water. *Geochim. et Cosmochim. Acta*, 6,
467 241-260.
- 468 Dansgaard, W. (1961). The isotopic composition of natural waters with special reference to the
469 Greenland Ice Cap. *Medd. Groenland*, 165, (2), 120 p.
- 470 Dansgaard, W. (1964). Stable isotopes in precipitation. *Tellus*, 6, 435-468.
- 471 Dobrowski, S. Z., Abatzoglou, J. T., Greenberg, J. A. & Schladow, S. G. (2009). How much
472 influence does landscape-scale physiography have on air temperature in a mountain
473 environment? *Agric. For. Meteorol.* 149, 1751-1758. doi:
474 10.1016/j.agrformet.2009.06.006
- 475 Duan, W., Ruan, J., Luo, W., Li., T., Tian, L., Zeng, G., et al. (2016). The transfer of seasonal
476 isotopic variability between precipitation and drip water at eight caves in the monsoon
477 regions of China. *Geochim. et Cosmochim. Acta*, 15, 250-266.
- 478 Easto, C.J. & Dettman, D.L. (2016). Isotope effects in hydrogeologic and climate reconstructions
479 of monsoon climates: Implications of some long-term data sets for precipitation. *Chem.*
480 *Geol.*, 430, 78-89.
- 481 Ehhalt, D., Knot, K., Nagel, J.F. & Vogel, J.C. (1963). Deuterium and oxygen 18 in rain water. *J.*
482 *Geophys. Res.*, 68, 3775-3780.

- 483 Epstein, S. (1956). Variations of the O18/O16 ratios of fresh water and Ice. Nat. Acad. Sci., Ncl.
484 Sci. Rep., 19, 20-25.
- 485 Epstein, S., & Mayeda, T. (1953). Variation on 18O content of waters from natural sources.
486 Geochim. et Cosmochim. Acta, 4, 213-214.
- 487 Friedman, I. (1953) Deuterium content of natural waters and other substances. Geochim. et
488 Cosmchim. Acta, 4, 89-103.
- 489 Friedman, I., G. I. Smith, J. Gleason, A. Warden, & J. M. Harris (1992). Stable isotope
490 composition of precipitation in southeastern California, 1, Modern precipitation. J.
491 Geophys. Res., 97, 5795-5812.
- 492 Friedman, I., Harris, J.M., Smith, G.I., Craig A. & Johnson, C.A. (2002a). Stable isotope
493 composition of waters in the Great Basin, United States 1. Air-mass trajectories. J.
494 Geophys. Res. Atmos., 107, (19). doi:10.1029/2001JD000565
- 495 Friedman, I., Smith, G.I., & Johnson, C.A., and Moscati, R.J. (2002b). Stable isotope
496 composition of waters in the Great Basin, United States, 2, Modern precipitation. J.
497 Geophys. Res., 107, (19), doi: 10.1029/2001JD000566.
- 498 Gat, J. (2001). Environmental isotopes in the hydrogeological cycle - Principles and applications.
499 IAEA, 2, 235 p.
- 500 Gilfillan, E.S. Jr. (1934). The isotopic composition of sea water. J. Am. Chem. Soc., 56, 406-
501 408.
- 502 Hager, G. & Foelsche, U. (2015). Stable isotope compositions of precipitation in Austria. Aust. J.
503 Earth Sci., 108, (2), 2-13.
- 504 Harada, M. & Titani, T. (1935). Isotopic composition of rain and snow water. Chem. Soc. Japan,
505 10, 206-263.
- 506 Houghton, J. G. (1969). Characteristics of rainfall in the Great Basin. Desert Res. Inst., Univ.
507 Nevada, Reno, Pub. 41054, 205 p.
- 508 Houghton, J.G. (1979). A model for orographic precipitation in the north-central Great Basin.
509 Monthly Weath. Rev., 107, 1462-1475.
- 510 IAEA (2021). Global network of isotopes in precipitation (GNIP). <https://nucleus.iaea.org/wiser>,
511 accessed March 21, 2021.
- 512 Jeton, A.E., Watkins, S.A., Lopes, T.J. & Huntington, J. (2005). Evaluation of Precipitation
513 Estimates from PRISM for the 1961-1990 and 1971-2000 Data Sets, Nevada. U.S. Geol.
514 Surv. Sci. Invest. Rpt. 2005-5291, 35 p.

- 515 Klaus, J., McDonnell, J., Jackson, R.C. & Griffiths, N. (2015). Where does stream water come
516 from in low-relief forested watersheds? A dual-isotope approach. *Hydrol. Earth Syst.*
517 *Sci.*, 19, (1), 125-35.
- 518 Kobayakawa, H.Y. & Horibe, Y. (1960). Deuterium abundance of natural waters. *Geochim. et*
519 *Cosmochim. Acta*, 20, 273-283.
- 520 Kurita, N., Fujiyoshi, Y., Nakayama, T., Matsumi, Y. & Kitagawa, H. (2014). Atmospheric
521 circulation controls on the inter-annual variability in precipitation isotope ratio in Japan.
522 *Climate Past Disc.*, 10 (5), 3989-4032.
- 523 Lewis, G.N. & Cornish, R. (1933). Separation of the isotopic forms of water by fractional
524 distillation. *J. Am. Chem. Soc.*, 55, 5061-5062.
- 525 Mantura, N.J. & Hare, S.R. (2002). The Pacific-Decadal Oscillation. *J. Ocean.*, 58, 35-44.
- 526 McEvoy, D.J., Mejia, J.F. & Huntington, J.L. (2014). Use of an observation network in the Great
527 Basin to evaluate gridded climatic data. *J. Hydrometeor.*, 5 (5) 1913-1931.
528 doi.org/10.1175/JHM-D-14-0015.1
- 529 Merlivant, L. & Jouzel, J. (1979). Global climatic interpretation of the deuterium-oxygen 18
530 relationship for precipitation. *J. Geophys. Res.*, 84. 5029-5033.
- 531 Michel, R.L., Jurgens, B.C. & Young, M.B. (2018). Tritium deposition in precipitation in the
532 United States, 1953-2013. *US Geol. Surv. Sci. Invest. Rpt.* 2018-5086, 12 p.
- 533 NOAA (2021). HYSPLIT a Hybrid Single-Particle Lagrangian Integrated Trajectory model.
534 www.noaa.gov/HYSPLIT_traj.php, accessed March 10, 2021.
- 535 Pape, J.R., Banner, J.L., Mack, L.E., Musgrove, M. & Guilfoyle, A. (2010). Controls on oxygen
536 isotope variability in precipitation and cave drip waters, central Texas, USA. *J. Hydrol.*,
537 385, 203-215.
- 538 Patrick, N. (2014). Evaluating near surface rates over complex terrain using an embedded
539 micrologger sensor network in Great Basin National Park. Ohio State University.
- 540 Rozanski, K., Araguas, L. & Gonfiantini, R. (1993). Isotopic patterns in modern global
541 precipitation, climate change in continental isotopic record. *Geophys. Monogr.* 78, 1-37.
- 542 Schell, W.R., Sauzay, G. & Payne, B.R. (1970). Tritium injection and concentration distribution
543 in the atmosphere. *J. Geophys. Res.* 75 (12), 2251-2266.
544 <https://doi.org/10.1029/JC075i012p02251>
- 545 Siegenthaler, U. & Oeschger, H. (1980). Correlation of ^{18}O in precipitation with temperature
546 and altitude. *Nature*, 285, 314-317.

- 547 Smith, K., Strong, C. & Shih-Yu Wang, S-Y (2015). Connectivity between historical Great
548 Basin precipitation and Pacific Ocean variability: A CMIP5 Model Evaluation. *J.*
549 *Climate*, 28, 15, 6092-6112. doi.org/10.1175/JCLI-D-14-00488.1
- 550 Smith, G. I., Friedman, I., Gleason, J. & Warden, A. (1992). Stable isotope composition of
551 ground waters in southeastern California, 2, Ground waters and their relation to modern
552 precipitation. *J. Geophys. Res.*, 97, 5813-5823
- 553 Suess, H.E. (1970). Transfer of carbon 14 and tritium from the atmosphere to the ocean. *J.*
554 *Geophys. Res.*, 75 (12), 2363–2364. <https://doi.org/10.1029/JC075i012p02363>.
- 555 Tes, R.V. (1939). Isotopic composition of rain water. *Akad. Nauk, USSR*, 23. 674.
- 556 Vuille, M. & Werner, M. (2005). Stable isotopes in precipitation recording South American
557 summer monsoon and ENSO variability: observations and model results. *Climate Dyn.*
558 25 (4), 401-413.
- 559 Yurtsever, Y. (1975). Worldwide survey of isotopes in precipitation. IAEA report, Vienna.
- 560 Wang, S.-Y., Gillies, R.R. & Reichler, T. (2012). Multidecadal drought cycles in the Great Basin
561 recorded by the Great Salt Lake: Modulation from a transition-phase teleconnection. *J.*
562 *Climate*, 25, 1711-1721. doi:10.1175/2011JCLI4225.1.
- 563 WRCC (2021). Western Regional Climate Center. <https://wrcc.dri.edu/summary/Climsmut.html>,
564 accessed February 18, 2021.
- 565 Wise, E. K. (2010). Spatiotemporal variability of the precipitation dipole transition zone in the
566 western United States. *Geophys. Res. Lett.* 37, L07706. doi:10.1029/2009GL042193
- 567 Yeh, H., Lin, H., Lee, C., Hsu, K. & Wu, C. (2014). Identifying seasonal groundwater recharge
568 using environmental stable isotopes. *Hydrology*, 6, 203-215.